Hybrid Inorganic−Organic Core−Shell Nanoparticles from Surface-Functionalized Titanium, Zirconium, and Vanadium Oxo Clusters

Guido Kickelbick,*,† Dieter Holzinger,† Chad Brick,† Gregor Trimmel,†,§ and Ellen Moons‡

Technische Universität Wien, Institut für Materialchemie, Getreidemarkt 9/153, A1060 Wien, Austria, and Department of Physics, Division for Engineering Sciences, Physics and Mathematics, Karlstad University, SE-651 88 Karlstad, Sweden

Received May 27, 2002. Revised Manuscript Received August 12, 2002

Novel surface-functionalized metal oxo clusters were obtained using an in situ surface-modification method based on the sol−gel process. A reaction of 2-bromoisobutyric acid with $Zr(OPr)_4$ or $Ti(O^iPr)_4$ resulted in the compounds $Zr_5O_4(BrC(CH_3)_2COO)_{10}(O^nPr)_2(^nPrOH)_4$ and $Ti_6O_4(BrC(CH_3)_2COO)_8(O^iPr)_8$. The reaction of 2-bromopropionic acid with $VO(O^iPr)_3$ resulted in the cluster $V_3O_3(BrC(CH_3)COO)_6(HO^iPr)$. All obtained compounds have in common that the organic functionalities are exclusively located on the surface of the well-defined sub-nanometer metal oxo clusters. The prepared compounds were successfully used as macro-initiators in atom transfer radical polymerizations (ATRP) and produced inorganic−organic core−shell nanoparticles.

Introduction

Inorganic−organic hybrid materials possess a huge potential in the synthesis of new functional materials. In particular, the combination of polyoxometalates with their unique properties for optical, electronic, or magnetic applications,[1] and organic polymers offer new possibilities in the design of materials through the combination of inorganic and organic systems. The inorganic moiety is commonly incorporated into such so-called nanocomposites applying molecular precursors either forming a network in a preformed polymer, for example, applying the sol−gel process, or in an in situ approach forming both the organic polymer and the inorganic species in one step.[2,3] An alternative approach is to incorporate preformed inorganic building blocks, which has the advantage that the compounds have a well-defined composition and morphology.[4] A major problem in the formation of such nanocomposites is the microphase separation. Therefore, compatibilization techniques for the interface between inorganic and organic moieties have to be applied to obtain more homogeneous materials. In most circumstances, the best method is the covalent linkage of the organic matrix to the inorganic particles by surface modification.[5] This methodology was applied for zirconium and titanium nanoclusters by an in situ formation of surface-functionalized clusters with unsaturated double bonds, which allow the cross-linking of these building blocks to organic monomers in polymerization reactions.[6−9] However, this technique has the disadvantage that the analysis and the controlled formation of, for example, thin films of such cross-linked materials is often not easy due to their insolubility and gumlike performance, depending on the degree of cross-linking. Therefore, a core−shell particle-like morphology is preferred due to easier handling and more straightforward analysis of the obtained systems by common particle characterization methods. A very convenient way to form such hybrid core−shell particles is the encapsulation of the inorganic core into a polymeric shell by grafting the polymers from the surface of the particles. This technique was already used for the formation of silica-based inorganic−organic core−shell systems.[10−14] In most of these cases controlled radical polymerization techniques

* To whom correspondence should be addressed. Fax: +43-1-58801-15399. E-mail: guido.kickelbick@tuwien.ac.at.
† Technische Universität Wien.
‡ Karlstad University.
§ Current address: Technische Universität Graz, Institut für Chemische Technologie Organischer Stoffe, Stremayrgasse 16, A8010 Graz, Austria.

(1) A good overview of the properties and applications of oxo metalate can be found in *Chem. Rev.* **1998**, *98* (1), 1−390.
(2) Sanchez, C.; Soler-Illia, G. J. d. A. A.; Ribot, F.; Lalot, T.; Mayer, C. R.; Cabuil, V. *Chem. Mater.* **2001**, *13*, 3061−3081.
(3) Kickelbick, G.; Schubert, U. *Monatsh. Chem.* **2001**, *132*, 13−30.
(4) Kickelbick, G. *Prog. Polym. Sci.* **2002**, in press.
(5) Kickelbick, G.; Schubert, U. In *Functionalization and Surface Treatment of Nanoparticles*; Barton, M.-I., Ed.; American Scientific Publishers: Stevenson Ranch, CA, 2002; in press.
(6) Schubert, U. *Chem. Mater.* **2001**, *13*, 3487−3494.
(7) Trimmel, G.; Fratzl, P.; Schubert, U. *Chem. Mater.* **2000**, *12*, 602−606.
(8) Trimmel, G.; Gross, S.; Kickelbick, G.; Schubert, U. *Appl. Organomet. Chem.* **2001**, *15*, 401−406.
(9) Trimmel, G.; Moraru, B.; Gross, S.; DiNoto, V.; Schubert, U. *Macromol. Symp.* **2001**, *175* (Polymerization Processes and Polymer Materials II), 357−366.
(10) von Werne, T.; Patten, T. E. *J. Am. Chem. Soc.* **1999**, *121*, 7409−7410.
(11) Tsujii, Y.; Ejaz, M.; Sato, K.; Goto, A.; Fukuda, T. *Macromolecules* **2001**, *34*, 8872−8878.
(12) Pyun, J.; Matyjaszewski, K.; Kowalewski, T.; Savin, D.; Patterson, G.; Kickelbick, G.; Hüsing, N. *J. Am. Chem. Soc.* **2001**, *123*, 9445−9446.
(13) Wurm, H. *Polym. Bull.* (*Berlin*) **2000**, *44*, 223−229.
(14) Costa, R. O. R.; Vasconcelos, W. L.; Tamaki, R.; Laine, R. M. *Macromolecules* **2001**, *34*, 5398−5407.

10.1021/cm021216y CCC: $22.00
Published on Web 10/01/2002

were used due to a precise control of the grafting process and the exclusive formation of polymer on the surface and not in solution, as is often the case in the initiation of free radical polymerizations. In this approach, usually silane coupling reagents with functional groups capable of initiating the polymerization were used for the surface modification.

In this paper we present the synthesis of novel well-defined organically functionalized metal oxo clusters of zirconium, titanium, and vanadium. The prepared systems were used as macroinitiators for atom transfer radical polymerization (ATRP). Applying this technique, we were able to extend the organic shell in a well-controlled manner.

Experimental Section

Measurements. NMR spectra were recorded on a 300-MHz DRX Avance Bruker or Bruker AC 250 instrument working at 300 (250) and 75.43 (66.9) MHz for ^{1}H and ^{13}C, respectively. Relative size exclusion chromatography (SEC) measurements in THF were performed using a Waters system including a Waters 515 HPLC pump, a Waters 717 autosampler, a Waters 2410 differential refractive index detector, and Styragel columns (HR 0.5, 3, and 4, linear) at 40 °C at a rate of 1 mL/min applying linear polystyrene standards. Molecular weight analysis was calculated with Waters Millennium[32] software including the GPC/V option and related to an internal standard (diphenyl ether). AFM measurements were carried out using a Digital Instruments Nanoscope IIIA Multimode. Light-scattering measurements were performed by applying a non-invasive backscattering technique by using an ALV-NIBS/HPPS instrument. TEM measurements were performed on a JEOL JEM-200CX instrument. Microanalyses were carried out by Microanalytical Laboratories, University of Vienna.

Materials. All chemicals were obtained from Aldrich. Cu(I)Br and Cu(I)Cl were stirred in glacial acetic acid overnight, filtered, and washed with absolute ethanol. Monomers were distilled from CaH_2, degassed, and stored in a refrigerator under an argon atomsphere prior to use. All other chemicals were used without further purification. All reactions were carried out under an argon atmosphere using Schlenk techniques.

Syntheses. *$Zr_5O_4(BrC(CH_3)_2COO)_{10}(O^nPr)_2(^nPrOH)_4$ (**1**).* A $Zr(OPr)_4$ (1.0 m, 2.23 mmol) solution was added to a solution of 1.52 mg (8.92 mmol) of 2-bromoisobutyric acid in 5 mL of propanol. After thorough mixing, colorless crystals precipitated from the solution within 5 days. These were isolated and dried. Yield: 850 mg (77%) of colorless crystals. Molecular weight: 2441.86. Calcd: C, 27.9; H, 4.0. Found: C, 26.1; H, 3.6. ^{1}H NMR (δ, $CDCl_3$, 22 °C): 6.17 (br, OH), 4.05 (m, 4 H, ZrOC**H**$_2$-CH_2CH_3), 3.80 (t, 8 H, coord. HOC**H**$_2CH_2CH_3$), 1.93, 1.91, 1.88 (s, 60.4 H, (C**H**$_3$)$_2$CBrCOOZr), 1.67 (m, 12 H, $ZrOCH_2C$**H**$_2CH_3$ and coord. $HOCH_2C$**H**$_2CH_3$), 0.87 and 0.79 (t, 18 H, $ZrOCH_2$-CH_2C**H**$_3$ and $HOCH_2CH_2C$**H**$_3$). ^{13}C NMR (δ, $CDCl_3$, 22 °C): 180.8 (br, COOZr), 176.3 (COOZr), 175.9 (COOZr), 73.0 ($ZrOCH_2CH_2CH_3$), 66.6 (coord. HO**C**$H_2CH_2CH_3$), 59.6, 59.2, and 58.8 (**C**Br$(CH_3)_2$COOZr), 31.3, 31.2, 30.8, and 30.7 (CBr-(**C**H_3)$_2$COOZr), 24.9 and 24.8 ($ZrOCH_2$**C**H_2CH_3 and coord. $HOCH_2$**C**H_2CH_3), 10.1 and 9.8 ($ZrOCH_2CH_2$**C**H_3 and coord. $HOCH_2CH_2$**C**H_3).

*$Ti_6O_4(BrC(CH_3)_2COO)_8(O^iPr)_8$ (**2**).* $Ti(O^iPr)_4$ (558 mg, 1.95 mmol) was added to 328 mg (1.95 mmol) of 2-bromoisobutyric acid in 5 mL of THF. After 48 h of stirring at room temperature, the solution was concentrated and rested in the refrigerator at 4 °C. After 3 weeks, colorless crystals were isolated. Yield: 310 mg (74%) of colorless crystals. Molecular weight: 2335.32. Calcd: C, 34.3; H, 4.8. Found: C, 34.6; H, 5.4. ^{1}H NMR (δ, $CDCl_3$, 22 °C): 4.75−4.11 (m, 4H, CH_3CH_2C**H**$_2$OTi), 2.00, 1.94, and 1.89 (s, 12 H, **(CH$_3$)$_2$**CBrCOOTi), 1.90−1.51 (m, 4 H, $TiOCH_2C$**H**$_2CH_3$), 1.07−0.81 (m, 6 H, $TiOCH_2$-CH_2C**H**$_3$). ^{13}C NMR (δ, $CDCl_3$, 22 °C): [179.5, 179.2, 177.7, 176.9] ($CBr(CH_3)_2$**C**OOTi), [82.3, 82.11, 82.07, 79.3, 79.1, 76.2, 76.1, 75.3] (TiO**C**$H_2CH_2CH_3$), [60.5, 59.9, 59.3, 58.8, 58.7] (**C**Br-$(CH_3)_2$COOTi), [31.9, 31.4, 31.3, 31.2, 31.1, 31.0] ($CBr($**C**$H_3)_2$-COOTi), [26.6, 26.1, 25.9, 25.8, 25.7, 25.6, 25.3, 25.2] ($TiOCH_2$-**C**H_2CH_3), [10.7, 10.5, 10.4, 10.2, 9.9] ($TiOCH_2CH_2$**C**H_3).

*$V_3O_3(BrCH(CH_3)COO)_6(HO^iPr)$ (**3**).* 2-Bromopropionic acid (2.838 g, 16.99 mmol) in 1 mL of 1-butanol was added to 1.029 g (4.24 mmol) of $VO(OiPr)_3$. The solution turned red after the addition. The solution was stirred at room temperature and rested in the refrigerator at 4 °C. After 2 days a precipitate, which was identified as vanadium oxide, and a few green crystals were isolated. ^{1}H NMR (δ, $CDCl_3$, 22 °C): 5.89 (b, −O**H**), 4.23 (m, 6 H, (CH_3)C**H**BrCOOV), 4.00 (m, 3 H, VOC**H**-**(**$CH_3)_2$), 1.78 (s, 18 H, VOCH(C**H$_3$)$_2$**), 1.21 (s, 18 H, C**H$_3$**CHBr). ^{13}C NMR (δ, $CDCl_3$, 22 °C): 175.0 (CHBR(CH_3)**C**OOV), 70.0 (O**C**H$(CH_3)_2$), 41.0 (**C**HBr(CH_3)COOV), 25.4 (CHBr(**C**$H_3)_2$-COOV), 21.9 (OCH(**C**$H_3)_2$).

X-ray Crystallography Study. Selected crystals were mounted on a Siemens SMART diffractometer with a CCD area detector. Graphite-monochromated Mo Kα radiation (71.073 pm) was used for all measurements. The nominal crystal-to-detector distance was 4.40 cm. A hemisphere of data was collected by a combination of three sets of exposures at 203 K. Each set had a different ϕ angle for the crystal, and each exposure took 20 s and covered 0.3° in ω. The data were corrected for polarization and Lorentz effects, and an empirical absorption correction (SADABS) was applied. The cell dimensions were refined with all unique reflections. The structures were solved by direct methods (SHELXS86). Refinement was carried out with the full-matrix least-squares method based on F^2 (SHELXL93) with anisotropic thermal parameters for all non-hydrogen atoms. Hydrogen atoms were inserted in calculated positions and refined riding with the corresponding atom. The Br positions of the 2-bromobutyrate ligands in **1** and **2** as well as the related positions in the 2-bromopropionate ligands in **3** are strongly disordered; therefore, a model of a 1/3 occupation of each of the atomic positions of the end group with bromine was applied in **1** and **2** and a 1/2 occupation in **3**. Table 1 shows the details of the crystal data and structure refinement.

Polymerizations. All polymerizations were carried out under an argon atmosphere using the freeze−pump−thaw technique for degassing the mixture following standard procedures for atom transfer radical polymerizations.[15]

Nanoparticle Characterization via AFM. The particles were cast on a mica substrate by leaving a drop of a dilute THF solution ($<10^{-5}$ M) of the material to evaporate spontaneously. Atomic force microscopy (AFM) was carried out on these substrates in tapping mode.

Results and Discussion

Formation of the Surface-Functionalized Metal Oxo Clusters. Metal alkoxides react with carboxylic acids to form surface-functionalized metal oxo clusters, which was already shown on different alkoxides/carboxylic acid systems.[3] A variety of different clusters with diverse morphologies and sizes have been obtained. In particular, the metal oxo clusters with polymerizable unsaturated bonds have attracted much interest because these systems can easily be incorporated into organic polymers.[6] The formation of the clusters is based on a three-step mechanism (Scheme 1): (i) substitution of alkoxide ligands by carboxylates, (ii) esterification of carboxylates by alcohol, and (iii) condensation of the fragments. We extended this so-called in situ approach to surface-functionalized metal oxo clusters using halogen-substituted carboxylic acids, which introduce reactive halogen atoms into the organic shell that can be

(15) Xia, J.; Matyjaszewski, K. *Macromolecules* **1997**, *30*, 7697−7700.

Table 1. Crystal Data and Structure Refinement

	1	2	3
empirical formula	$C_{58}H_{42}Br_{10}O_{30}Zr_5$	$C_{54}H_{56}Br_{10}O_{34}Ti_6$	$C_{21}H_{25}Br_6O_{16}V_3$
formula weight	2441.86	2335.32	1165.69
crystal system	monoclinic	monoclinic	triclinic
space group	$P2(1)/n$	$P2(1)/n$	$P\bar{1}$
unit cell dimensions (pm, deg)	1853.36(10)	1277.81(7)	1096.7(2)
	2191.45(11)	1523.75(8)	1212.6(2)
	2269.35(11)	2277.64(12)	1737.8(3)
	90.00	90.00	107.372(4)
	91.208(1)	104.784(1)	98.015(4)
	90.00	90.00	99.125(4)
volume (pm^3)	$9215.0(8) \times 10^6$	$4287.9(4) \times 10^6$	$2134.5(7) \times 10^6$
Z	4	4	2
calculated density ($g\ cm^{-1}$)	1.802	1.724	1.814
absorption coefficient (mm^{-1})	5.118	4.519	6.313
$F(000)$	4765	2175	1116
crystal size (mm)	$0.48 \times 0.38 \times 0.20$	$0.44 \times 0.36 \times 0.34$	$0.22 \times 0.18 \times 0.10$
θ range for data collection (deg)	1.44−21.97	1.63−23.26	1.83−21.18
limiting indices	$-19 \le h \le 19$	$-14 \le h \le 12$	$-10 \le h \le 11$
	$0 \le k \le 23$	$-16 \le k \le 16$	$-11 \le k \le 12$
	$0 \le l \le 23$	$-20 \le l \le 25$	$-17 \le l \le 17$
reflections collected/unique	37999/11249	19722/6138	7704/4575
	[R(int) = 0.0525]	[R(int) = 0.0353]	[R(int) = 0.0769]
completeness to max. θ	99.9	99.7	97.4
max. and min. transmission	0.4275	0.3087	0.5709
	0.1926	0.2411	0.3372
data/restraints/parameters	11249/0/936	6138/0/482	4575/0/416
goodness-of-fit on F^2	1.034	1.053	1.104
final R indices [$I > 2\sigma(I)$]	R1 = 0.0950, wR2 = 0.2390	R1 = 0.0585, wR2 = 0.1658	R1 = 0.1204, wR2 = 0.3105
R indices (all data)	R1 = 0.1173, wR2 = 0.2611	R1 = 0.0739, wR_2 = 0.1787	R1 = 0.2223, wR2 = 0.3690
extinction coefficient	0.00017(6)	0.0003(2)	0.0045(17)
largest diff. peak and hole ($e \cdot A^{-3}$)	5.104 and −4.303	1.027 and −0.794	2.221 and −1.304
weighting scheme[a] x/y	0.1177/287.96	0.1216/2.32 P	0.2/0

[a] $W = 1/[\sigma^2(F_o^2) + (xP)^2 + yP]$, $P = (\mathrm{Max}(F_o^2,0) + 2F_c^2)/3$.

Scheme 1

(i) Substitution

$$(RO)_4M + HOOC{\sim\sim}FG \rightleftharpoons (RO)_{4-m}M[OOC{\sim\sim}FG]_m + m\ ROH$$

(ii) Esterification (formation of water)

$$ROH + HOOC{\sim\sim}FG \rightleftharpoons ROOC{\sim\sim}FG + H_2O$$

(iii) Condensation

$$(RO)_{4-m}M[OOC{\sim\sim}FG]_m + H_2O \rightleftharpoons M_wO_x(OR)_y(OOC{\sim\sim}FG)_z$$

M: Metal
FG: Functional group

used for initiating ATRP. In this study 2-bromoisobutyric acid was used in reactions with $Zr(O^nPr)_4$ and $Ti(O^iPr)_4$ and 2-bromopropionic acid was used in a reaction with $VO(O_iPr)_3$.

The reaction of $Zr(O^nPr)_4$ with 4 equiv of 2-bromoisobutyric acid results in the zirconium oxo cluster $Zr_5O_4(BrC(CH_3)_2COO)_{10}(OPr)_2(PrOH)_4$ (**1**), which is obtained as colorless crystals. The single-crystal X-ray analysis reveals a molecular structure (Figure 1) containing a Zr_5 cluster core. Selected bond lengths and angles are presented in Table 2. The five Zr atoms form a square pyramidal arrangement in which four of the five faces are capped by μ_3 oxygen atoms. The coordination environment of the Zr atoms is not uniform; while Zr(1), Zr(3), and Zr(5) are coordinated by eight oxygens, Zr(2) and Zr(4) show only a coordination sphere of seven. The metal oxo core of the present structure shows similarities to the already known compound $Zr_6(OH)_4O_4(OMc)_{12}$[16] (OMc = methacrylate). The latter has an octahedral arrangement of the six Zr atoms, which are also bridged by μ oxygen or hydroxy functions. The

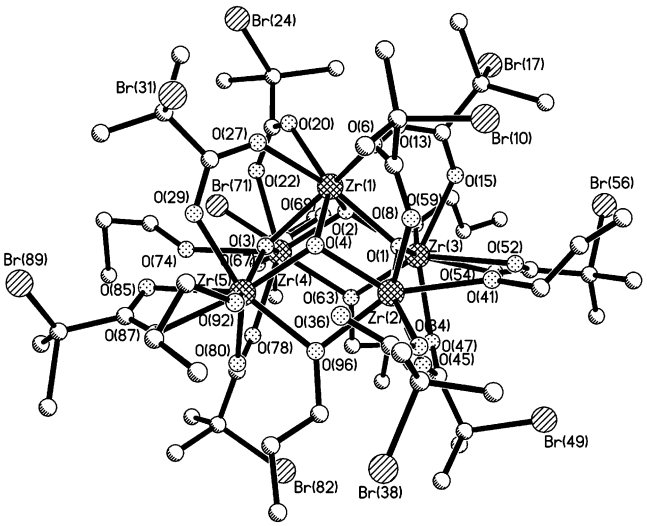

Figure 1. Molecular structure of $Zr_5O_4(BrC(CH_3)_2COO)_{10}(O^nPr)_2(^nPrOH)_4$ (**1**). H atoms and labels of the C atoms are omitted for clarity.

structure presented in this paper can in principle be formed from the Zr_6 core, eliminating one metal corner. All ZrO coordination polyhedra share one edge with adjacent polyhedra in the basal position of the pyramidal arrangement and one of the apical [ZrO_8] polyhedra (Figure 2).

The Zr atoms are either bridged by μ_2-O^nPr or by carboxylate groups. Contrary to other zirconium clusters in the presented structure, not all carboxylate groups are bonded in a bridging or chelating manner; there are also two η^1-coordinated ligands (Zr(2) and Zr(4)). In addition, every basal Zr atom is coordinated by one

(16) Kickelbick, G.; Schubert, U. *Chem. Ber.* **1997**, *130*, 473−477.

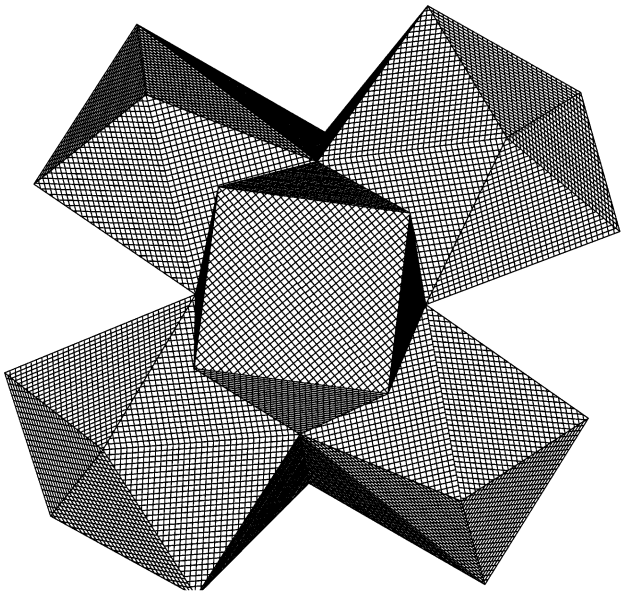

Figure 2. Linking of the coordination polyhedra in $Zr_5O_4(BrC(CH_3)_2COO)_{10}(O^nPr)_2(^nPrOH)_4$ (**1**).

Table 2. Selected Bond Lengths (pm) and Angles (deg) for $Zr_5O_4(BrC(CH_3)_2COO)_{10}(O^nPr)_2(^nPrOH)_4$ (1)

Zr(1)−O(1)	215.2(9)	Zr(4)−O(2)	202.9(10)
Zr(1)−O(2)	213.3(9)	Zr(4)−O(3)	205.3(9)
Zr(1)−O(3)	216.8(9)	Zr(5)−O(3)	205.6(9)
Zr(1)−O(4)	214.3(9)	Zr(4)−O(22)	216.6(11)
Zr(1)−O(6)	225.9(9)	Zr(4)−O(63)	215.9(10)
Zr(1)−O(13)	223.8(10)	Zr(4)−O(67)	218.7(12)
Zr(1)−O(20)	224.5(10)	Zr(4)−O(74)	231.6(11)
Zr(1)−O(27)	223.6(10)	Zr(4)−O(78)	218.1(12)
Zr(1)−Zr(2)	330.40(18)	Zr(5)−O(4)	205.9(9)
Zr(1)−Zr(3)	336.00(18)	Zr(5)−O(29)	217.8(10)
Zr(1)−Zr(4)	330.70(18)	Zr(5)−O(80)	217.8(11)
Zr(1)−Zr(5)	336.87(19)	Zr(5)−O(87)	223.4(12)
Zr(2)−O(1)	205.5(9)	Zr(5)−O(85)	260.7(16)
Zr(2)−O(4)	202.9(9)	Zr(5)−C(86)	279.0(2)
Zr(2)−O(8)	215.1(9)	Zr(5)−O(92)	228.6(9)
Zr(2)−O(34)	215.0(10)	Zr(5)−O(96)	220.4(10)
Zr(2)−O(41)	230.4(10)		
Zr(2)−O(45)	216.9(10)	Zr(1)−O(1)−Zr(2)	103.5(4)
Zr(2)−O(96)	216.5(10)	Zr(2)−O(1)−Zr(3)	142.8(5)
Zr(2)−Zr(5)	344.65(19)	Zr(1)−O(1)−Zr(3)	105.8(4)
Zr(3)−O(1)	206.0(8)	Zr(1)−O(2)−Zr(4)	105.2(4)
Zr(3)−O(2)	207.2(9)	Zr(1)−O(2)−Zr(3)	106.1(4)
Zr(3)−O(15)	217.9(9)	Zr(3)−O(2)−Zr(4)	115.2(5)
Zr(3)−O(47)	218.3(11)	Zr(4)−O(3)−Zr(5)	143.8(5)
Zr(3)−O(52)	258.0(14)	Zr(1)−O(3)−Zr(4)	103.1(4)
Zr(3)−C(53)	278.0(18)	Zr(1)−O(3)−Zr(5)	105.7(4)
Zr(3)−O(54)	224.5(11)	Zr(1)−O(4)−Zr(2)	104.7(4)
Zr(3)−O(59)	227.1(10)	Zr(1)−O(4)−Zr(5)	106.6(4)
Zr(3)−O(63)	219.7(10)	Zr(2)−O(4)−Zr(5)	114.9(4)
Zr(3)−Zr(4)	346.32(19)		

propanol ligand. The mean Zr−O distance of the latter ligands is 230 pm and therefore typical for coordinating propanol molecules compared to propoxy groups, which show usually a smaller Zr−O distance. Although we did not succeed in localizing the propanol H atom from the X-ray data, the short O(36)−O(92) and O(59)−O(69) distances of 266.3 and 262.6 pm indicate a hydrogen bridge between the propanol ligand and the η^1-coordinated carboxylate ligands. A similar stabilization is possible between the chelating carboxylate O atom and the other propanol groups (O(41)−O(52): 265.3 pm; O(74)−O(85): 266.0 pm). The Br atoms in the functional $CBrMe_2$ groups are statistical disordered and are all

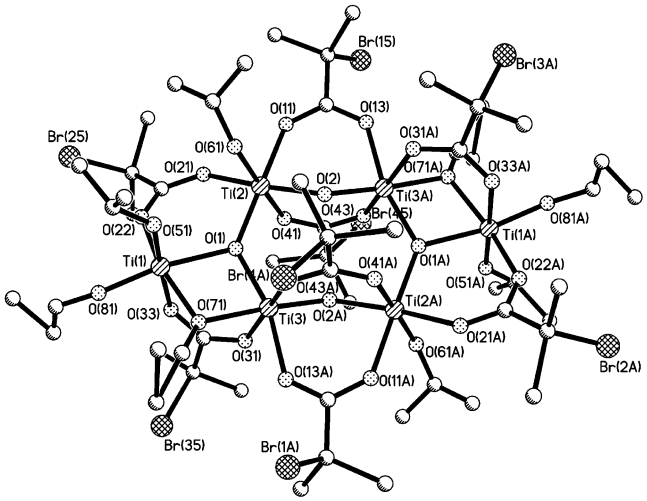

Figure 3. Molecular structure of $Ti_6O_4(BrC(CH_3)_2COO)_8(O^iPr)_8$ (**2**). H atoms and labels of the C atoms are omitted for clarity. The structure also contains solvent molecules that were also omitted.

Table 3. Selected Bond Lengths (pm) and Angles (deg) for $Ti_6O_4(BrC(CH_3)_2COO)_8(O^iPr)_8$ (2)[a]

Ti(1)−O(51)	177.9(4)	Ti(3)−O(71)	204.2(3)
Ti(1)−O(71)	195.7(4)	Ti(3)−O(2A)	175.9(3)
Ti(1)−O(81)	177.8(4)	Ti(3)−O(13A)	205.9(4)
Ti(1)−O(1)	210.7(3)	Ti(3)−O(43A)	200.8(4)
Ti(1)−O(22)	202.9(4)	Ti(3)−Ti(2A)	337.01(12)
Ti(1)−O(33)	219.0(4)	Ti(3A)−O(2)	175.9(3)
Ti(1)−Ti(3)	308.87(13)	Ti(3A)−O(13)	205.9(4)
Ti(3)−O(1)	188.9(3)	Ti(3A)−O(43)	200.8(4)
Ti(2)−O(1)	189.7(3)		
Ti(2)−O(2)	187.2(3)	Ti(2)−O(1)−Ti(3)	130.43(17)
Ti(2)−O(11)	209.8(4)	Ti(1)−O(1)−Ti(3)	101.09(14)
Ti(2)−O(21)	206.7(4)	Ti(1)−O(1)−Ti(2)	127.21(17)
Ti(2)−O(41)	210.2(4)	Ti(2)−O(2)−Ti(3A)	136.31(19)
Ti(2)−O(61)	176.2(4)	Ti(1)−Ti(3)−Ti(2A)	159.83(4)
Ti(2)−Ti(3A)	337.01(12)	Ti(1)−O(71)−Ti(3)	101.11(15)
Ti(3)−O(31)	200.3(4)	Ti(3)−O(71)	204.2(3)

[a] All atoms marked with an A were generated through symmetry operations. Mechanism of the formation of oxo metalate clusters.

available for further reactions due to their peripheral positions.

From the reaction of $Ti(O^iPr)_4$ with 1 equiv of 2-bromoisobutyric acid in THF $Ti_6O_4(BrC(CH_3)_2COO)_8(O^iPr)_8$ (**2**) is formed as colorless crystals. A single-crystal X-ray analysis resulted in the molecular structure shown in Figure 3. Selected bond lengths and angles of this structure are listed in Table 3.

All Ti atoms are located in a planar arrangement and reveal an octahedral coordination sphere of oxygen atoms. The assembly of the cluster core as well as the propoxide and carboxylate groups is similar to the already known structures $Ti_6O_4(OAc)_8(OPr)_8$,[17] $Ti_6O_4(OMc)_8(OPr)_8$,[17] and $Ti_6O_4(OMc)_8(OEt)_8$.[18] The connection of the $[TiO_6]$ octahedra is much more open than that in the Zr_5 structure (Figure 4). Four of the six octahedra share an edge with adjacent ones, while the others are only connected via two corners. Bridging between the Ti atoms occurs via μ_2 and μ_3 oxygen atoms, via μ_2 propoxide bridges, or via carboxylate groups

(17) Peterlik, H. *Chem. Mater.* **2002**, *14*, 2732−2740.
(18) Schubert, U.; Arpac, E.; Glaubitt, W.; Helmerich, A.; Chau, C. *Chem. Mater.* **1992**, *4*, 291−295.

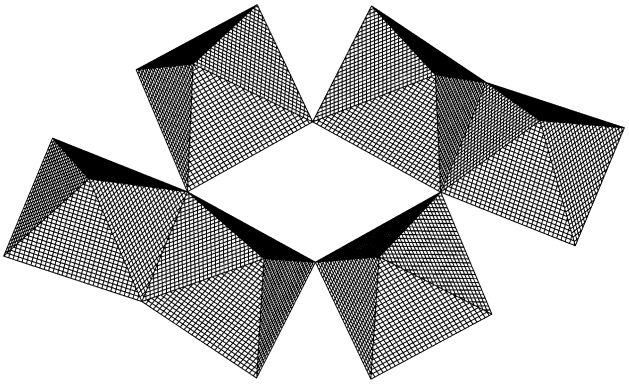

Figure 4. Linking of the coordination polyhedra in $Ti_6O_4(BrC(CH_3)_2COO)_8(O^iPr)_8$ (**2**).

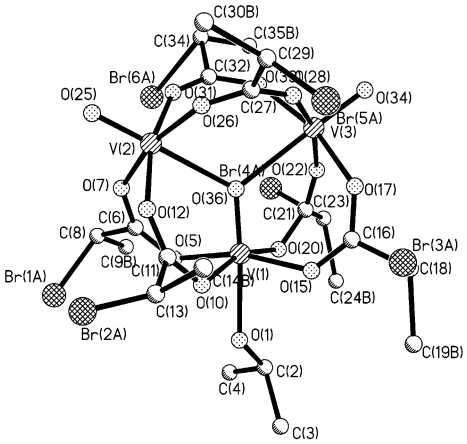

Figure 5. Molecular structure of $V_3O_3(BrC(CH_3)COO)_6(HO^iPr)$ (**3**). H atoms and labels of the C atoms are omitted for clarity.

coordinating adjacent Ti atoms in a bridging manner. Similar to the Zr_5 structure, the Br atoms in the functional $CBrMe_2$ groups are statistically disordered and are all available for further reactions due to their peripheral positions.

The reaction of 2-bromoisobutyric acid with Ti or Zr alkoxides in ratios other than those mentioned above did not result in crystallization and attempts to characterize the solution structures of the resulting molecules with other methods have not yet succeeded. These systems are currently under investigation using extended X-ray absorption fine structure (EXAFS) studies in solution.

In a similar approach, 2-bromopropionic acid was added in a 4-fold excess to $VO(O^iPr)_3$ and the crystalline compound $V_3O_3(BrC(CH_3)COO)_6(HO^iPr)$ (**3**) was isolated in low yields. The obtained vanadium oxo cluster contains only V(IV) while the oxidation state in the precursor was V(V). The oxidized species in the reaction mixture was not identified. The vanadium oxo cluster contains three octahedral-coordinated vanadium atoms bridged by a central μ_3 oxygen atom and six 2-bromopropionate ligands (Figure 5). Selected bond lengths and angles are given in Table 4. A similar structural pattern has already been observed in the literature; the carboxylates in these related structures were benzoic acid[19] or propionic acid.[20] Two of the three vanadium atoms show the typical V−O distance of a double-bonded

Table 4. Selected Bond Lengths (pm) and Angles (deg) for $V_3O_3(BrC(CH_3)COO)_6(HO^iPr)$ (3)

V(1)−O(5)	1.953(16)	O(25)−V(2)−O(31)	97.2(8)
V(1)−O(15)	1.941(16)	O(25)−V(2)−O(12)	99.5(8)
V(1)−O(36)	1.621(12)	O(31)−V(2)−O(12)	163.2(7)
V(1)−O(1)	2.136(15)	O(25)−V(2)−O(26)	97.2(8)
V(1)−O(10)	1.958(16)	O(31)−V(2)−O(26)	93.3(8)
V(1)−O(20)	1.977(15)	O(12)−V(2)−O(26)	86.2(8)
V(2)−O(7)	1.997(18)	O(25)−V(2)−O(7)	98.0(8)
V(2)−O(12)	1.980(19)	O(31)−V(2)−O(7)	84.2(7)
V(2)−O(25)	1.575(14)	O(12)−V(2)−O(7)	91.9(7)
V(2)−O(26)	1.987(19)	O(26)−V(2)−O(7)	164.8(7)
V(2)−O(31)	1.94(2)	O(25)−V(2)−O(36)	179.1(7)
V(2)−O(36)	2.375(12)	O(31)−V(2)−O(36)	82.8(6)
V(3)−O(17)	1.960(15)	O(12)−V(2)−O(36)	80.5(6)
V(3)−O(34)	1.550(14)	O(26)−V(2)−O(36)	81.9(6)
V(3)−O(22)	1.955(16)	O(7)−V(2)−O(36)	82.9(6)
V(3)−O(28)	1.949(18)	O(34)−V(3)−O(28)	97.4(8)
V(3)−O(33)	2.016(19)	O(34)−V(3)−O(22)	96.8(7)
V(3)−O(36)	2.384(13)	O(28)−V(3)−O(22)	165.8(7)
		O(34)−V(3)−O(17)	97.7(7)
O(5)−V(1)−O(15)	164.3(7)	O(28)−V(3)−O(17)	85.4(7)
O(5)−V(1)−O(10)	91.9(7)	O(22)−V(3)−O(17)	91.9(6)
O(5)−V(1)−O(36)	96.4(7)	O(34)−V(3)−O(33)	98.0(8)
O(5)−V(1)−O(20)	87.2(7)	O(28)−V(3)−O(33)	93.4(8)
O(10)−V(1)−O(15)	88.2(6)	O(22)−V(3)−O(33)	85.4(7)
O(10)−V(1)−O(20)	162.7(7)	O(17)−V(3)−O(33)	164.3(7)
O(10)−V(1)−O(36)	96.4(7)	O(34)−V(3)−O(36)	178.4(7)
O(15)−V(1)−O(20)	88.1(6)	O(28)−V(3)−O(36)	84.2(6)
O(15)−V(1)−O(36)	99.1(7)	O(22)−V(3)−O(36)	81.6(5)
O(20)−V(1)−O(36)	100.9(6)	O(17)−V(3)−O(36)	82.1(5)
O(1)−V(1)−O(5)	82.0(7)	O(33)−V(3)−O(36)	82.2(6)
O(1)−V(1)−O(10)	78.3(7)	V(1)−O(36)−V(2)	123.5(7)
O(1)−V(1)−O(15)	82.6(6)	V(1)−O(36)−V(3)	121.0(6)
O(1)−V(1)−O(20)	84.5(6)	V(2)−O(36)−V(3)	115.5(5)
O(1)−V(1)−O(36)	174.4(6)		

oxygen atom pointing outwards of the cluster core (V(2)−O(25) 157.5(14) pm and V(3)−O(34) 155.0(14) pm). The third vanadium atom is linked to a similar oxygen atom; however, this atom is directed to the center of the V_3 triangle. The V(1)−O(36) distance is longer compared to the others (1.621(12) pm), which is the result of the interaction with the additional vanadium atoms. The coordination sphere of V(1) is saturated by a coordinating ^{i}PrOH group, which was clearly identified by ^{1}H NMR measurements. The $[VO_6]$ octahedra are sharing only one corner, namely, the central μ_3 oxygen atom (Figure 6).

The obtained structures show that the in situ formation of surface-functionalized metal oxo clusters by the reaction of carboxylic acids and metal alkoxides seems to be a general approach to such types of materials.

Polymerization Reactions. Most of the published examples of the preparation of inorganic−organic core−shell-type nanoparticles by applying a "grafting from" approach are based on amorphous silica cores, which were functionalized after synthesis with organically modified silanes.[10,12] Contrarily, the method presented in this paper allows an in situ process for the preparation of well-defined, monodisperse, surface-functionalized metal oxo clusters. The largest diameters of the initiating molecules measured metal-to-metal distances are 336.9, 902.3, and 353.7 pm for the zirconium, titanium, and vanadium oxo cluster, respectively. As observed in the molecular structures all bromine groups of the surface-functionalized zirconium, titanium, and vanadium oxo clusters are accessible for further reac-

(19) Cotton, F. A.; Lewis, G. E.; Mott, G. N. *Inorg. Chem.* **1982**, *21*, 3127.

(20) Huang, X. *Chin. J. Struct. Chem. (Jiegou Huaxue)* **2000**, *19*, 326.

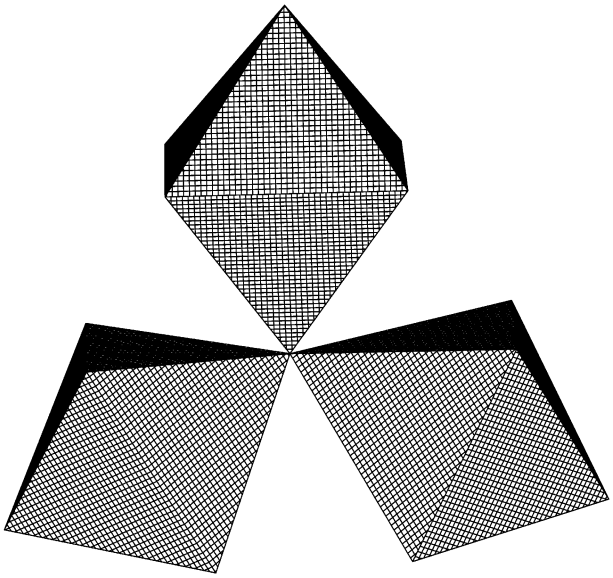

Figure 6. Linking of the coordination polyhedra in $V_3O_3(BrC(CH_3)COO)_6(HO^iPr)$ (**3**).

Scheme 2

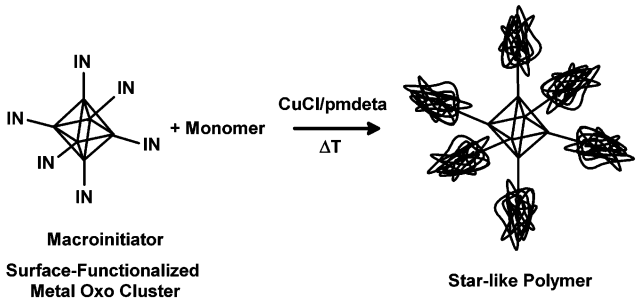

tions due to their peripheral positions. Esters of 2-bromoisobutyric acid or 2-bromopropionic acid as pure organic initiators have already been used for ATRP reactions with several vinyl monomers.[21−23] The clusters obtained in this study are potential macroinitiators for starlike polymers that possess six, eight, or ten initiating groups depending on the cluster type. The ability to use these surface-functionalized metal oxo clusters as macroinitiators in the copper-mediated ATRP of methyl methacrylate and styrene for ATRP was therefore investigated. As active metal species in the polymerizations, a 1:1 mixture between CuCl or CuBr and *N*,*N*,*N*′,*N*″,*N*″-pentamethyldiethylenetriamine (pmdeta) was applied. In preliminary experiments the parameters of the polymerizations such as temperature, amount of solvent, and ratio between initiating sites and metal species were optimized. The degree of polymerization was calculated for a molecular weight of 2000 per potential initiating site.

We were able to apply all obtained clusters as macroinitiators in ATRP reactions (Scheme 2). The polymerization reactions showed a high degree of control. As a representative example, cluster **1** is discussed in more detail. Cluster **1** showed the highest degree of control

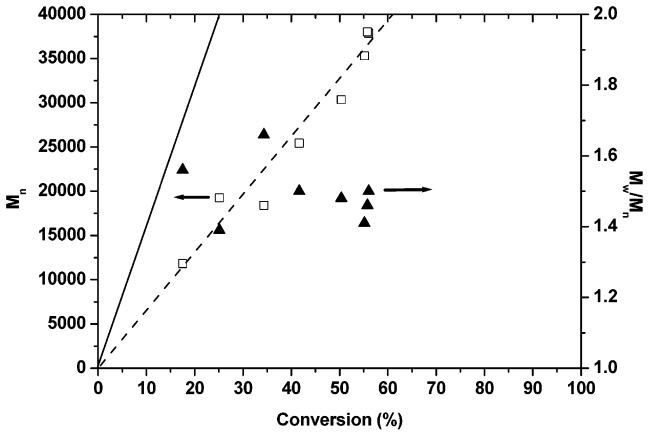

Figure 7. Evolution of molecular weight (□) and molecular weight distribution, M_w/M_n (▲), on monomer conversion for the MMA polymerization initiated by $Zr_5O_4(BrC(CH_3)_2COO)_{10}(O^n\text{-}Pr)_2(^nPrOH)_4$ (**1**). $[M]_0$:$[I]_0$:[CuCl/pmdeta] = 2000:1:1; volume MMA:toluene = 1:1. The straight line is the expected molecular weight evolution while the dotted line is a linear fit through the determined data points.

(lowest polydispersity) in the polymerization of MMA at a temperature of 75 °C, an initiating site to CuCl/pmdeta ratio of 1:0.5, and a solvent-to-monomer volume ratio of 1:1 using toluene as the solvent. Under these conditions a total molecular weight of the system of 38 000 with a polydispersity of 1.46 was reached after 24 h of reaction time and 56% conversion. The SEC chromatogram showed a monomodal molecular weight distribution. The zirconium cluster was also used in the polymerization of styrene, which was carried out with CuBr instead of CuCl due to the higher reactivity of the bromide. With use of the same conditions as those in the polymerization of MMA, the reaction was much slower, which is based on the lower reactivity of styrene. After 72 h of reaction time only 15% conversion was observed (M_n = 13 800, PDI = 1.28). Hence, in additional polymerization experiments the temperature was raised to 90 °C and the initiator-to-metal complex ratio was changed to 1:1. When these conditions were applied, the conversion after 72 h was 41% (M_n = 25 200, PDI = 1.46).

To prove that the polymerizations occur in a controlled manner, kinetic studies were carried out. Figure 7 shows the evolution of the molecular weight of the polymer on monomer conversion as determined by SEC for the MMA polymerization initiated by cluster **1**. ATRP as a controlled polymerization reaction should have a linear dependence of the evolution of molecular weight throughout the reaction time. However, the evolution of the molecular weight is lower than theoretically expected. This can be attributed partly to the SEC measurement, which was done in relation to a linear polystyrene standard that does not represent the hydrodynamic volume of a particle-like structure very well. The evolution of the molecular weight distribution (M_w/M_n), with polydispersities higher in the beginning and steadily decreasing throughout the reaction, is typical for ATRP reactions. Additionally, the kinetics plot shows the characteristically first-order dependence of the reaction concerning the monomer concentration, which is represented by the linear fit of $\ln([M]_0/[M])$ vs time plot in Figure 8. In summary, it can be concluded that

(21) Wang, J.-S.; Matyjaszewski, K. *Macromolecules* **1995**, *28*, 7901−7910.
(22) Matyjaszewski, K.; Wei, M.; Xia, J.; McDermott, N. E. *Macromolecules* **1997**, *30*, 8161−8164.
(23) Zhang, X.; Xia, J.; Gaynor, S. G.; Matyjaszewski, K. *Polym. Mater. Sci. Eng.* **1998**, *79*, 409−410.

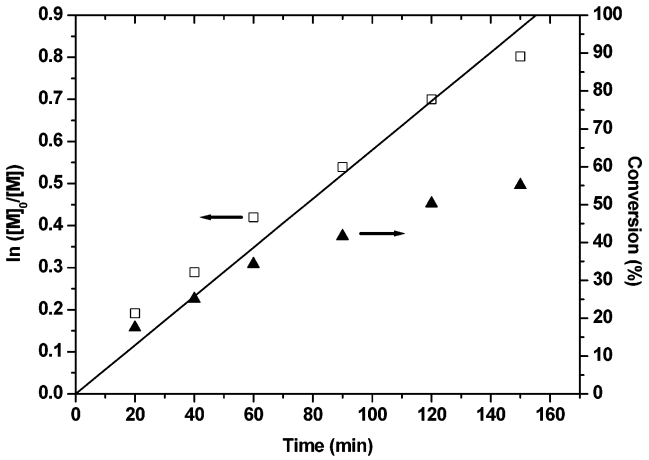

Figure 8. Kinetic plot for the MMA polymerization initiated by $Zr_5O_4(BrC(CH_3)_2COO)_{10}(O^nPr)_2(^nPrOH)_4$ (**1**). $[M]_0$:$[I]_0$:[CuCl/pmdeta] = 2000:1:1; volume MMA:toluene = 1:1.

the reaction is controlled and that termination reactions such as particle coupling do obviously occur rarely.

One of the advantages of the ATRP method is that the formed polymers contain a Br atom at the end of the chain. After isolation, the polymers can therefore be applied again as initiators for polymerization reactions. This was also proved with the obtained materials. After isolation the Zr_5/PMMA core−shell system was, for example, chain extended with *tert*-butyl methacrylate and methacryloxypropyltrimethoxysilane. The polymerizations were carried out under similar conditions as the polymerizations of the first block. However, in both chain extensions a temperature of 90 °C and CuBr as the copper halide were used. The isolated particulate Zr_5/PMMA macroinitiator had a molecular weight of 38 000 and a molecular weight distribution of 1.46. The SEC study after the chain extension revealed for the *tert*-butyl methacrylate polymerization an increase of the molecular weight to 49 400 after 72 h. This is equal to a conversion of 9.3% of the monomer, also confirmed by ^{1}H NMR studies. The molecular weight distribution remained low with $M_w/M_n = 1.66$. The conversion of methacryloxypropyltrimethoxysilane after the same time was 17.8%. However, a reliable SEC analysis of the resulting polymer was not possible due to cross-linking reactions of the trimethoxysilane groups during chromatography. The resulting particle is an interesting precursor for further sol−gel reactions due to the trialkoxy end groups.

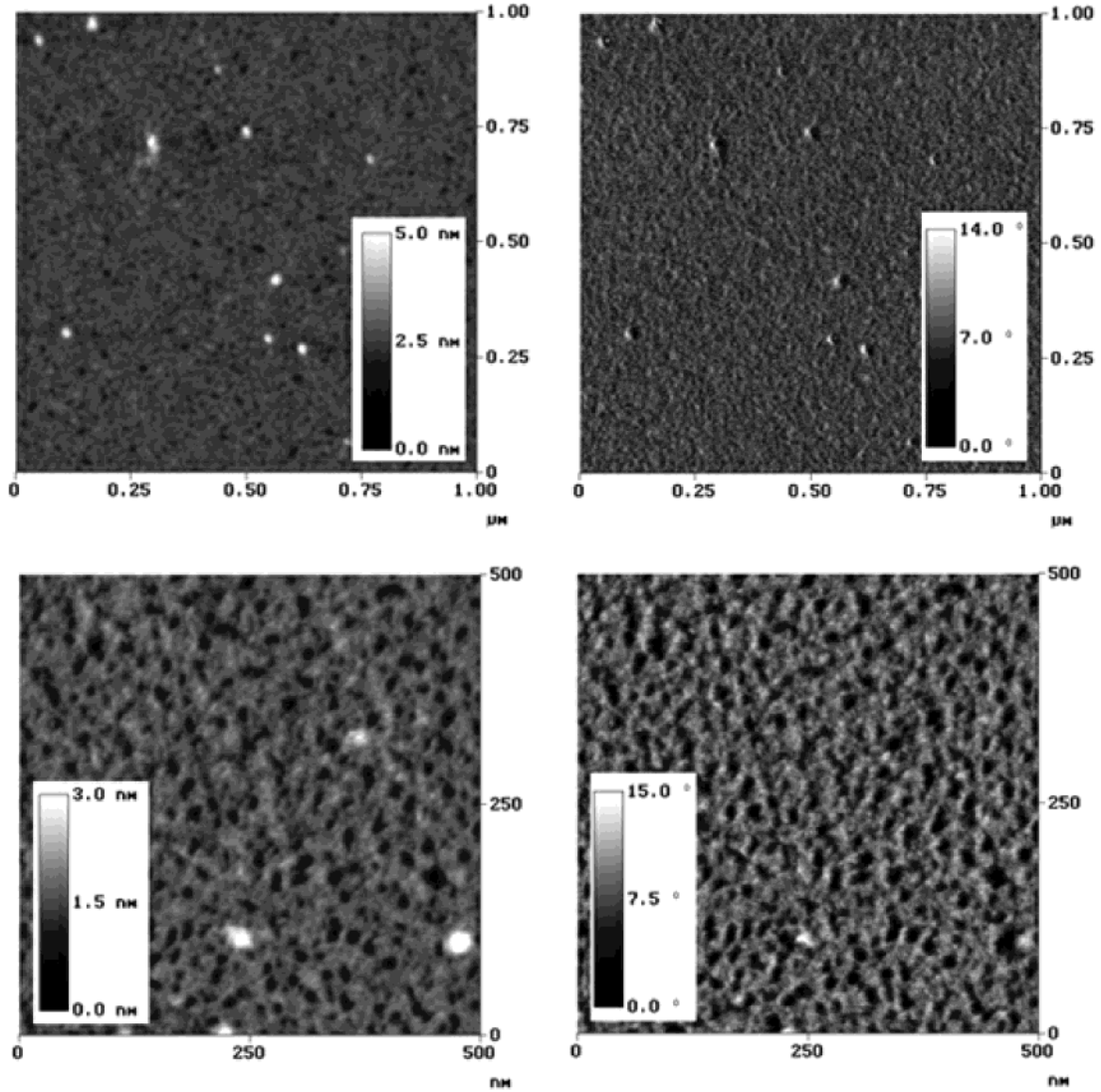

Figure 9. AFM height (left) and phase (right) images obtained in tapping mode for a thin film of ZrO_5/PMMA deposited from a THF solution on mica. Scan sizes are 1 × 1 μm (top) and 500 × 500 nm (bottom) and *z*-scales are indicated.

Nanoparticle Characterization. The size of the nanoparticles was determined by applying noninvasive backscattering and AFM imaging. The results of these measurements are exemplarily shown using the Zr_5/PMMA particles. Light scattering was carried out in THF at 25 °C and data analysis was performed using an integral-type function to the correlation function by a constrained regularization method.[24] Zr_5/PMMA nanoparticles (M_w = 38 000; PDI = 1.46) showed a number-weighted diameter of 6.0 ± 0.4 nm. If the samples rested for several hours, an agglomeration was observed in the solution. The agglomerates had a medium diameter of several tens of nanometers. They grew steadily with increasing time. However, the weight number of the agglomerates was small compared to the other particles and reached a maximum of 5% number weighted after 1 day.

Casted films were imaged by atomic force microscopy (AFM) in tapping mode, yielding a topographic height image as well as a phase image. Phase images are able to reveal differences in mechanical properties due to interactions between the tip and the sample. In the topographic images of Zr_5/PMMA nanoparticles islands of about 20 ± 5 nm in diameter and 1−2 ±0.2 nm in height, dispersed in a homogeneous background, were observed. After longer drying times the background showed also a more distinct pattern on the nanometer scale. The contrast observed in the phase images is weak, which indicates that the nanoparticles are covered by polymer so that the tip did not detect any mechanical differences on the surface. Figure 9 shows AFM height (left) and phase (right) images of the ZrO_5/PMMA systems with 1 × 1 μm (top) and 500 × 500 nm (bottom) scan sizes.

The results of the AFM studies reveal that the particles form islands of agglomerated particles when the casting method is applied. Provided that the particles form monolayers on the support, the height can give a hint on their diameter, which is in the observed case approximately half the diameter reached by the light scattering technique. A possible reason for this behavior is the fact that the measurements in THF represent the swollen state of the polymer attached to the cluster surface, while the AFM studies reveal the dried particles on a support. Furthermore, the polymer layer can spread on the surface of the support.

Routine transmission electron microscopy techniques were also applied in the characterization of the particles. The polymer shell was destroyed in the electron beam by applying these techniques and therefore we were not able to prove the core−shell structure of the particles. However, more sophisticated electron microscopy studies are currently under investigation.

Conclusions

Novel types of zirconium, titanium, and vanadium metal oxo clusters were obtained by the reaction of the metal alkoxides with an excess of 2-bromoisobutyric acid or 2-bromopropionic acid. The obtained surface-functionalized compounds have a core−shell structure in which the core is built up of different types of connected [MO_x] polyhedra and the shell consists of the bromocarboxylate groups. The halogen atoms are therefore fully accessible for further reactions. This was shown in using these compounds as multiarm macroinitiators for ATRP. The resulting core−shell nanoparticles were characterized by light scattering and AFM and revealed diameters in the nanometer region.

Acknowledgment. We like to thank Dr. Michael Puchberger for his technical assistance concerning NMR measurements. We thank the Fonds zur Förderung der wissenschaftlichen Forschung, Austria, and the European Cooperation in the Field of Scientific and Technical Research (COST) Action D19 for their support of this work.

Supporting Information Available: X-ray structural information on **1**−**3** as an X-ray crystallographic file (CIF). This material is available free of charge via the Internet at http://pubs.acs.org.

CM021216Y

(24) Schätzel, K. *Appl. Phys.* **1987**, *B42*, 193−213.